Time-dependent Ginzburg-Landau simulations of the voltage-current characteristic of type-II superconductors with pinning

T. Winiecki and C. S. Adams
Department of Physics, University of Durham, Durham DH1 3LE, United Kingdom
(Received 9 October 2001; published 28 February 2002)

The dynamics of vortices in a type-II superconductor with defects is studied by solving the time-dependent Ginzburg-Landau equations in two and three dimensions. We show that vortex flux tubes are trapped by volume defects up to a critical current density where they begin to jump between pinning sites along static flow channels. We study the dependence of the critical current on the pinning distribution and find for random distributions a maximum critical current equal to 2% of the depairing current at a pinning density 3 times larger than the vortex line density, whereas for a regular triangular pinning array the critical current is greater than 7% of the depairing current when the pinning density matches the vortex line density.

DOI: 10.1103/PhysRevB.65.104517 PACS number(s): 74.60.Ge, 74.76.−w

I. INTRODUCTION

In a type-II superconductor, dissipation is associated with the motion of the vortex lattice.[1,2] This dissipation is reduced by the presence of defects, which pin the vortex lattice up to a critical current density where depinning occurs. In many applications such as superconducting magnets, one is interested in optimizing the vortex pinning to achieve the maximum critical current. However, the details of the depinning transition are complex, involving the nonequilibrium dynamics of an elastic lattice through a disordered medium. Theoretical studies based on molecular dynamics simulations suggest the existence of various dynamical phases of vortex motion including plastic flow, uncoupled static channels, and coupled channels.[3,4] It is also possible to simulate vortex dynamics by solving the time-dependent Ginzburg-Landau (TDGL) equations,[5–9] where the vortex-vortex interaction is completely characterized by the Ginzburg-Landau parameter κ. However, TDGL simulations of the voltage-current (V-I) characteristic of a three-dimensional superconductor with finite κ are computationally intensive, in part because the standard explicit integration methods require very small time steps. Although more efficient semi-implicit methods are widely used to simulate the $\kappa\rightarrow\infty$ limit[9] and analogous problems such as three-dimensional vortex dynamics in superfluids,[10] they are not widely used for the more general finite-κ system. Consequently, previous studies of the effect of pinning on the V-I curve have been restricted to single pinning sites,[7] and the dependence of the critical current on the density and distribution of pinning sites has not been studied.

In this paper we employ a semi-implicit method to solve the TDGL equations in two and three dimensions for any κ.[11] For intermediate values of κ, our semi-implicit scheme is two orders of magnitude faster than explicit methods. We employ three-dimensional simulations to gain qualitative insight into the depinning transition and two-dimensional simulations to make quantitative measurements of the V-I curve and the dependence of the critical current on the density and distribution of pinning sites. Although pinning may arise due to magnetic defects, dislocations, grain boundaries, and correlated disorder such as twin planes in high-T_c superconductors, we restrict the current study to volume defects which exclude the supercurrent.

The paper is arranged as follows: In Sec. II we outline the TDGL model used to simulate vortex motion and calculate the V-I characteristic. In Sec. III we present the results of the three-dimensional simulations. In Sec. IV we study vortex motion in two dimensions and show how the breakdown of superconductivity occurs via channeled vortex flow. In Sec. V we present V-I curves for a two-dimensional superconducting slab. In Sec. VI, we study the dependence of the critical current on the density and distribution of pinning sites. Finally, we summarize the main results in Sec. VII.

II. TIME-DEPENDENT GINZBURG-LANDAU EQUATIONS

In the Ginzburg-Landau model, a superconductor is characterized by a complex order parameter ψ. The local density of superconducting electrons is represented by $|\psi|^2$. The theory postulates that close to the critical temperature, the free energy can be expanded in a series of the form

$$\mathcal{F}(\psi,\nabla\psi,\boldsymbol{A},\nabla\times\boldsymbol{A}) = a|\psi|^2 + \frac{1}{2}b|\psi|^4 + \frac{\hbar^2}{2m_s}\left|\left(\nabla - \mathrm{i}\frac{e_s}{\hbar}\boldsymbol{A}\right)\psi\right|^2 + \frac{1}{2\mu_0}|\nabla\times\boldsymbol{A} - \mu_0\boldsymbol{H}|^2, \quad (1)$$

where a and b are phenomenological constants that depend on external parameters such as temperature, $\boldsymbol{A}$ denotes the vector potential, $\boldsymbol{H}$ an external magnetic field, and e_s and m_s are the effective charge and the effective mass of the Cooper pairs. Below the transition temperature T_c, a becomes negative, whereas $b>0$ for all T.

The time-dependent Ginzburg-Landau equations are obtained from the free energy functional by assuming that the order parameter relaxes towards an energy minimum with a rate proportional to the gradient of the free energy. Including an electric potential Φ to retain the gauge invariance of the equations, one obtains[12]

$$\frac{\hbar^2}{2m_s D}\left(\partial_t + \mathrm{i}\frac{e_s}{\hbar}\Phi\right)\psi = \frac{\hbar^2}{2m_s}\left(\nabla - \mathrm{i}\frac{e_s}{\hbar}\boldsymbol{A}\right)^2\psi + |a|\psi - b|\psi|^2\psi, \tag{2}$$

$$\frac{1}{\mu_0}\nabla\times(\nabla\times\boldsymbol{A} - \mu_0\boldsymbol{H}) = \boldsymbol{j}, \tag{3}$$

where D is a phenomenological diffusion constant. Equation (3) is the Maxwell equation for the magnetic field, where the displacement current $\epsilon_0\dot{\boldsymbol{E}}$ has been neglected.[13] The total current $\boldsymbol{j}$ is given by the sum of the supercurrent,

$$\boldsymbol{j}_s = \frac{\hbar e_s}{2m_s \mathrm{i}}(\psi^*\nabla\psi - \psi\nabla\psi^*) - \frac{e_s^2}{m_s}|\psi|^2\boldsymbol{A}, \tag{4}$$

and the normal current given by Ohm's law,

$$\boldsymbol{j}_n = \sigma(-\nabla\Phi - \partial_t\boldsymbol{A}), \tag{5}$$

where σ is the conductivity. We scale the length in multiples of the coherence length, $\xi = \hbar/\sqrt{2m|a|}$; time in $\tau = \xi^2/D$; the order parameter in $\psi_0 = \sqrt{|a|/b}$; the vector potential in $A_0 = \sqrt{2}\kappa H_c\xi$ where $H_c = \mu_0|a|^2/b$; the electric potential in $\Phi_0 = (\xi/\tau)A_0$; and conductivity in units of the normal conductivity $\sigma_0 = 1/\kappa^2 D\mu_0$. The so-called Ginzburg-Landau parameter is given by $\kappa^2 = 2m^2 b/e^2\hbar^2\mu_0$. The characteristic length scale for variations of the magnetic field is $\lambda = \kappa\xi$, and $\nabla\times\boldsymbol{A}$ measures the magnetic field in units of $\sqrt{2}\kappa H_c = H_{c2}$. The Meissner-state critical field is given by $H_c = 1/\sqrt{2}\kappa$ and the depairing current density[1] by $j_D = 2/3\sqrt{3} = 0.385$. In scaled units Eqs. (2) and (3) become

$$(\partial_t + \mathrm{i}\Phi)\psi = (\nabla - \mathrm{i}\boldsymbol{A})^2\psi + \psi - |\psi|^2\psi, \tag{6}$$

$$\kappa^2\nabla\times\nabla\times\boldsymbol{A} = (\nabla S - \boldsymbol{A})|\psi|^2 + \sigma(-\nabla\Phi - \partial_t\boldsymbol{A}) + \kappa^2\nabla\times\boldsymbol{H}, \tag{7}$$

where S denotes the phase of ψ. The last term in Eq. (7) can be understood as an external current $\boldsymbol{j}_{ext}$ with $\nabla\boldsymbol{j}_{ext} = 0$ and can be used to model external fields or magnetic impurities in the material.

The measurable quantities $\boldsymbol{E}$, $\boldsymbol{B}$, $|\psi|^2$, and $\boldsymbol{j}$ are invariant under the transformation

$$\boldsymbol{A} \to \boldsymbol{A} + \nabla\Lambda,$$

$$\psi \to \psi\mathrm{e}^{\mathrm{i}\Lambda},$$

$$\Phi \to \Phi - \dot{\Lambda}, \tag{8}$$

where Λ is an arbitrary scalar field. We choose the zero potential gauge $\Lambda(\boldsymbol{r},t) = \int dt\Phi(\boldsymbol{r},t)$, in other words, $\Phi(\boldsymbol{r}) \equiv 0$ at all times.[14] For this choice, Eqs. (6) and (7) become

$$\partial_t\psi = (\nabla - \mathrm{i}\boldsymbol{A})^2\psi + \psi - |\psi|^2\psi, \tag{9}$$

$$\sigma\partial_t\boldsymbol{A} = (\nabla S - \boldsymbol{A})|\psi|^2 - \kappa^2\nabla\times(\nabla\times\boldsymbol{A} - \boldsymbol{H}). \tag{10}$$

Note that although the scalar potential no longer appears explicity in the equations, a potential and a normal current still arise through the time dependence of the vector potential, as apparent from Eq. (5).

The dynamics of the superconductor depends only on the dimensionless parameters κ and σ. In Ref. 11, we suggest a fast and reliable numerical method to find an approximate solution to Eqs. (9) and (10) for intermediate values of κ. Here we report results for the case of $\kappa = 3$ and 5 with $\sigma = 1$. The equations are discretized using a grid of $51\times51\times51$ points with a grid spacing $h = 0.4$. The gauge invariance of the discretized equations is preserved by introducing link variables following the method of Refs. 14 and 15. The discretized equations are solved using a semi-implicit Crank-Nicholson method with a time step $\delta t = 0.5$. A current flow along x is induced by imposing a magnetic field difference ΔB_z between the upper ($y = 10$) and lower ($y = -10$) boundaries. The supercurrent across the boundary is set to zero. We impose periodic boundary conditions at $x = \pm 10$ and $z = \pm 10$. The average current density is given by $j = \kappa^2\Delta B_z/d$, where d is the width of the superconductor. A pinning array is produced by adding a potential term to Eq. (1) consisting of a random distribution of cubic potential steps with side length $a = 1.2$ and height $V_0 = 5.0$. In agreement with other studies,[16] we find that the pinning strength increases with a for $a < \xi$ and saturates for $a > \xi$. A more sophisticated pinning model would be needed to account for the large pinning forces observed for small defects.[17]

III. VORTEX LATTICE MOTION IN THREE DIMENSIONS

Figure 1 shows a sequence of images illustrating the motion of the vortex lattice through the pinning array. Only a small section ($9\times7\times20$ coherence lengths with 12 pinning sites) of the complete simulation ($20\times20\times20$ coherence lengths with 40 pinning sites) is shown. In frame 1, six flux tubes are visible. By comparing frames 1, 2, and 3, one sees that the central flux tubes are moving whereas the two pairs on either side are pinned. However, between frames 4 and 5 the flux tubes on the left and right jump to the next pinning site. This differential motion between neighboring planes in the vortex lattice plays an important role in the voltage-current characteristic (see below). After frame 6, a similar but not identical sequence recurs. For the simulations presented in Fig. 1, the bending of the vortex lines is increased by the choice of a larger value of κ and strong pinning. However, no entangling of vortex lines is observed. For smaller κ, the vortex lines become more rigid, and the behavior of the three-dimensional system and a two-dimensional cross section are qualitatively very similar.

IV. VORTEX LATTICE MOTION IN TWO DIMENSIONS

We use two-dimensional simulations to study the effect of pinning on the voltage-current characteristic or *V-I* curve of a superconductor with $\kappa = 3$, where three-dimensional effects are suppressed. In addition, we reduce the size and strength of the pinning sites to $a = 0.8$ and $V_0 = 2.0$, respectively. In Fig. 2 we present contour plots illustrating the vortex lattice in two dimensions. Figure 2(a) shows the instantaneous vortex distribution for a perfect superconductor (no pinning). The vortex density is proportional to the magnetic field which decreases linearly from the bottom to the top. The

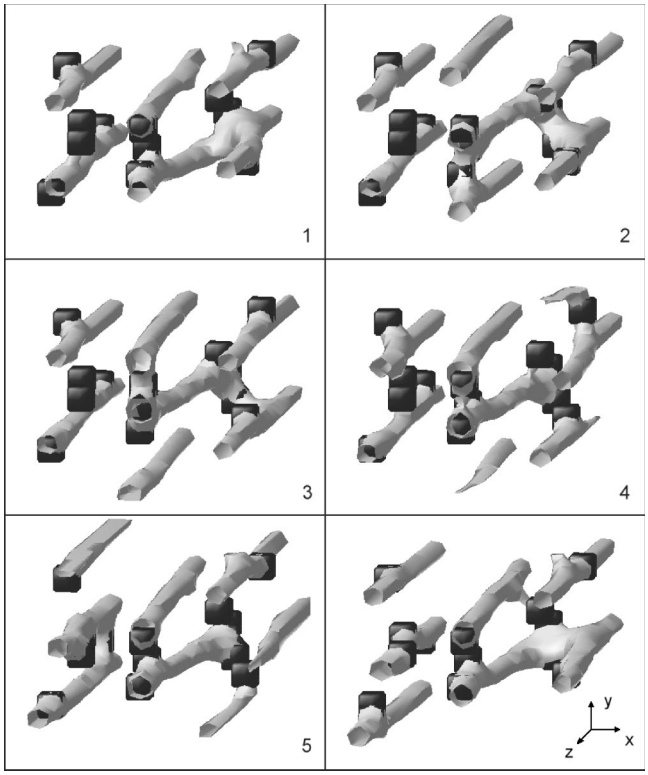

FIG. 1. A sequence of three-dimensional images showing the motion of a $\kappa=5$ vortex lattice through a random pinning array. Only a subregion (dimensions $9\times7\times20$ coherence lengths) of the total simulation is shown. Twelve pinning sites indicated by black cubes (not to scale) are visible. The axes are shown inset in frame 6. The current flows along *x*, the external magnetic field is along *z*, and the vortices move in the $-y$ direction. The external magnetic field and current are $B_{\rm ext}=0.4$ and $j=5\times10^{-3}$, respectively. The gray flux tubes correspond to surfaces of constant supercurrent density, $|\psi|^2=0.05$. The time interval between successive frames is 100.

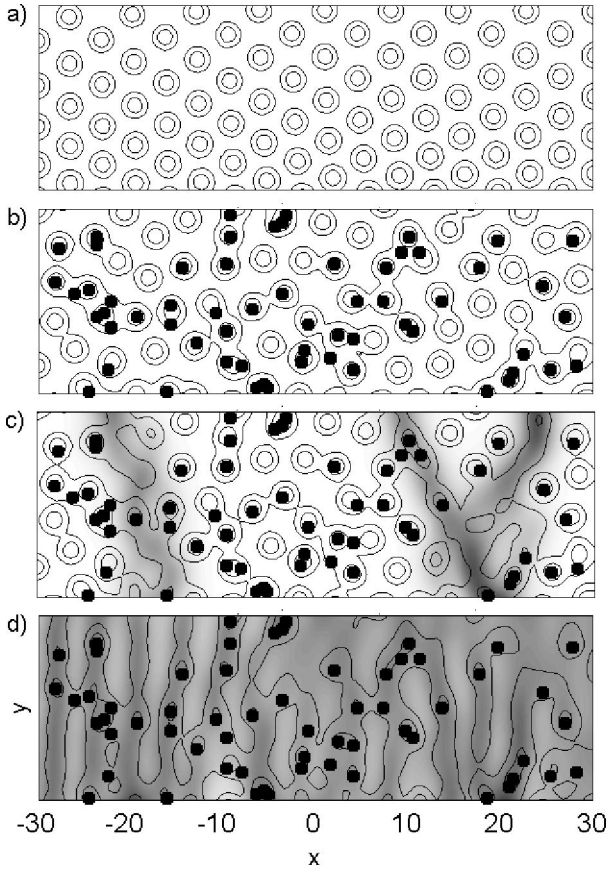

FIG. 2. Contour plots of the supercurrent density for a section of a superconductor with dimensions 60×20 coherence lengths, and $\kappa=3$, subject to an external magnetic field in the *z* direction, $B_{\rm ext}=0.4$. The current flows in the *x* direction and the vortices move in the *y* direction. (a) For a current $j=0.06$ and no pinning, the vortices form a triangular lattice with lattice spacing proportional to the local magnetic field. (b) The addition of pinning (density 0.056 ξ^{-2}) creates a vortex glass, which at low currents $j=0.004$ is pinned. (c) At intermediate currents $j=0.005$, vortex motion begins along channels, indicated by the gray scale image of the local electric field, superimposed on a time-averaged contour plot of the supercurrent density. (d) At larger currents $j=0.011$, all the vortices are moving and the electric field is nonzero everywhere; however, the channels, where vortex motion mainly occurs, are still visible.

vortices move upwards with a speed $v=E/B$, where B is the local magnetic field and the electric field E is constant throughout the sample.

Adding defects transforms the triangular lattice into an irregular vortex glass, Fig. 2(b). For low driving fields, the vortex glass is frozen. As the current is increased, individual vortices begin to jump between pinning sites. The motion is indicated in Fig. 2 by showing the local electric field, $\boldsymbol{E}=-\partial_t\boldsymbol{A}$, using a gray scale (darker indicating higher field). As in the three-dimensional simulations, Fig. 1, the motion begins along channels. The existence of static channels confirms the results of molecular dynamics simulations.[3,4] In the Ginzburg-Landau model channels can merge or divide at intermediate drive currents, as shown in Fig. 2(c). At larger currents, all the vortices are moving but the channels are still evident, Fig. 2(d).

V. *V-I* CURVES

The onset of vortex motion coincides with the onset of dissipation or breakdown of superconductivity. In Fig. 3 we plot the *V-I* curve for a two-dimensional thin film for different defect densities. The voltage is measured by decreasing the current at a very slow rate of -1.2×10^{-7}, and the *V-I* curves are obtained from a 200-point moving average. As our sample size is relatively small, surface effects tends to dominate. The critical current due to the Bean-Livingston barrier for vortices entering and leaving the calculation region[5] is the same order of magnitude as the pinning effect. In order to study pinning only we remove the surface effects by adding a boundary layer of width 9ξ on either side of a calculation regoin with width 30ξ. Within the boundary layer, a linear ramp potential reduces the supercurrent density gradually to zero. The current density and the voltage are measured within the calculation region ($|y|\leqslant15$) only.

The shape of the *V-I* curve is dependent on the details of the vortex dynamics. The characteristic ''curved foot'' can be explained by the combination of an increase in the number of

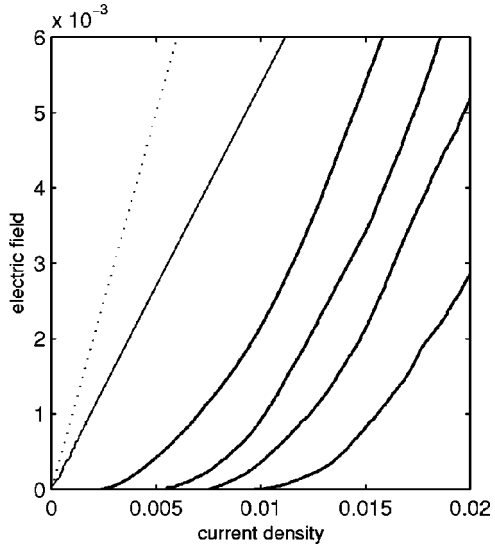

FIG. 3. The *V-I* curves for a two-dimensional section of superconductor with pinning densities (from the right) $0.14\xi^{-2}$, $0.28\xi^{-2}$, $0.39\xi^{-2}$, and $0.56\xi^{-2}$ (at these relatively high densities, the critical current decreases with increasing pinning density). The thin black line corresponds to the *V-I* curve without pinning, and the dotted line shows the normal resistance $\sigma E = j$. Note that at large currents the slope of the *V-I* curves is similar to the normal resistance curve.

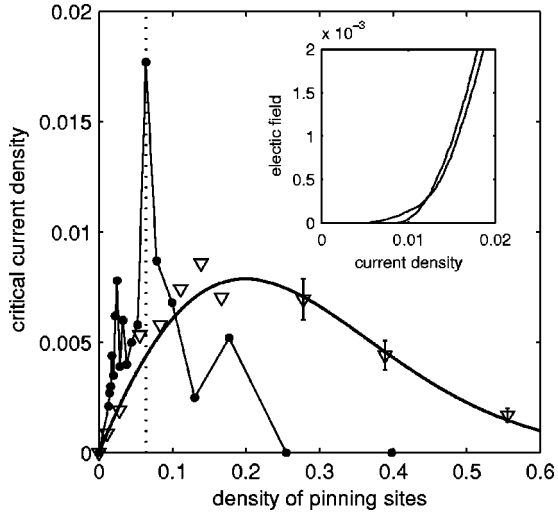

FIG. 4. The critical current density as a function of the defect density (in units of ξ^{-2}) for both random distributions (∇) and regular triangular arrays ($\bullet$). The data points are determined from an average of six random distributions. The error bars (shown for the high density distribution only) indicate the standard deviation. An example illustrating the effect of the distribution on the *V-I* curves is shown inset. The bold curve is a fit using the function $Ax\exp(-Bx)$, where A and B are fit parameters. The critical current density for a regular triangular array is a maximum when the pinning density is equal to vortex line density (indicated by the dotted line).

vortex flow channels and increased flow along each active channel, as illustrated in Figs. 2(c) and 2(d). The *V-I* curve becomes linear when all the vortices start to move. The ratio between the *V-I* curves and the normal resistance (the dotted line in Fig. 3) gives the dimensionless resistivity, which measures the fraction of current carried by normal electrons.

VI. CRITICAL CURRENT

As the current is decreased the voltage becomes zero; i.e., all the vortices become pinned, at some finite current which we define as the critical current density j_c. In the absence of finite-temperature-induced fluctuations or vortex creep, the value of j_c is well defined. However the critical current is sensitive to the exact distribution of pinning sites; therefore, we average over six random distributions with the same density. Figure 4 shows a plot of the average value of j_c against pinning density. The maximum critical current density is about 2% of the depairing current j_D. For comparison, the optimum critical current density of Nb-Ti alloy is $\sim 3\%$ of j_D; however, three-dimensional simulations and a different value of the conductivity parameter σ are needed to make a direct quantitative comparison. The maximum value of j_c occurs at pinning density about 3 times larger than the vortex line density (indicated by the dotted line in Fig. 4).

The dependence of the critical current on the defect density fits reasonably well to a function of the form $Ax\exp(-Bx)$. The linear increase at low pinning density follows from the linear dependence of the critical current on the pinning force. The exponential decrease at large pinning densities is due to the competing effect of supercurrent depletion by defects. The shape of the curve and the relatively high optimum pinning density also agree qualitatively with experimental results on silver doped high-T_c superconductors.[18]

For certain random distributions one finds persistence static channels which can dramatically reduce the critical current. This is illustrated in Fig. 4 (inset), where the curve with lower dissipation at large currents has a significantly lower critical current.

One approach to increase the critical current is to fabricate a regular pinning array.[19–21] In Fig. 4 we show that a regular triangular array increases the critical currents by more than a factor of 2; however, the optimum pinning density is sharply peaked around the vortex line density. Consequently, the enhancement is only obtained within a narrow range of the external magnetic field. This agrees with experimental studies where a sharp enhancement peak is obtained at matching magnetic field values.[21] There are two additional critical current peaks, one at one-third the vortex line density where every third vortex is trapped (illustrated in Fig. 5) and one at half the vortex line density, which is weaker because the matching only occurs on alternate planes. For small pinning sites ($a = 0.8$ compared to the vortex cores size of 2) the maximum critical current is about 5% of the depairing current j_D. For $a = 2$ we obtain $j_c = 0.074 j_D$, which suggests that other pinning mechanisms may be needed to obtain $j_c \sim j_D$.

VII. SUMMARY

In summary, we have studied vortex dynamics in two- and three-dimensional superconductors by solving the time-

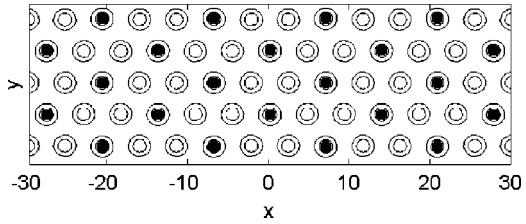

FIG. 5. Contour plots of the supercurrent density for a section of a superconductor with dimensions 60×20 coherence lengths and $\kappa=3$, subject to an external magnetic field $B_{\text{ext}}=0.4$ in the z direction. For a current, $j=0.06$, the vortex lattice remains pinned by the defect array.

dependent Ginzburg-Landau equations. We introduce pinning sites by adding localized potential terms which deplete the supercurrent and study the effect of pinning on the voltage-current characteristic of the superconductor. We show that the breakdown of superconductivity is associated with the appearance of channeled vortex flow, providing an independent check of the results of molecular dynamics simulations. The characteristic curved foot in the *V-I* curve arises due to the combination of the formation of more channels and faster vortex flow along each channel. We use the simulations to make a quantitative prediction of the critical current in two dimensions for the particular case where the dimensionless Ginzburg-Landau and conductivity parameters are $\kappa=3$ and $\sigma=1$, respectively. For a random pinning array, we find a maximum critical current equal to 2% of the depairing current occurring at a pinning density of about 3 times the vortex line density. For a regular pinning array we find a critical current greater than 7% of the depairing current at the vortex matching magnetic field. However, these results suggest that additional pinning mechanisms such as magnetic defects are required to explain the large critical observed in some experiments. Further work is needed to include magnetic defects into the TDGL model.

ACKNOWLEDGMENTS

We thank S. J. Bending for comments. Financial support was provided by the EPSRC.

[1] M. Tinkham, *Introduction to Superconductivity*, 2nd ed. (McGraw-Hill, New York, 1996).
[2] Y. B. Kim, C. F. Hempstead, and A. R. Strnad, Phys. Rev. **139**, A1163 (1965).
[3] K. Moon, R. T. Scalettar, and G. T. Zimanyi, Phys. Rev. Lett. **77**, 2778 (1996).
[4] C. J. Olson, C. Reichhardt, and F. Nori, Phys. Rev. Lett. **81**, 3757 (1998).
[5] R. Kato, Y. Enomoto, and S. Maekawa, Phys. Rev. B **47**, 8016 (1993).
[6] M. Machida and H. Kaburaki, Phys. Rev. Lett. **71**, 3206 (1993).
[7] M. Machida and H. Kaburaki, Phys. Rev. B **50**, 1286 (1994).
[8] Q. Du, M. D. Gunzburger, and J. S. Peterson, Phys. Rev. B **51**, 16 194 (1995).
[9] I. Aranson, A. Koshlev, and V. Vinokur, Phys. Rev. B **56**, 5136 (1997).
[10] T. Winiecki and C. S. Adams, Europhys. Lett. **52**, 257 (2000); M. Leadbeater, T. Winiecki, D. C. Samuels, C. F. Barenghi, and C. S. Adams, Phys. Rev. Lett. **86**, 1410 (2001).
[11] T. Winiecki and C. S. Adams, cond-mat/0106466 (unpublished).
[12] M. Cyrot, Rep. Prog. Phys. **36**, 103 (1973).
[13] L. P. Gor'kov and N. B. Kopnin, Usp. Fiz. Nauk **116**, 413 (1975) [Sov. Phys. Usp. **18**, 496 (1976)].
[14] H. Frahm, S. Ullah, and A. T. Dorsey, Phys. Rev. Lett. **66**, 3067 (1991).
[15] W. D. Gropp, H. G. Kaper, G. K. Leaf, D. M. Levine, M. Palumbo, and V. M. Vinokur, J. Comput. Phys. **123**, 254 (1996).
[16] G. Stejic, L. D. Cooley, R. Joynt, D. C. Larbalestier, and S. Takacs, Supercond. Sci. Technol. **5**, S176 (1992).
[17] E. V. Thuneberg, J. Kurkijarvi, and D. Rainer, Phys. Rev. Lett. **48**, 1853 (1982).
[18] N. Savvides, A. Katsaros, and S. X. Dou, Physica C **179**, 361 (1991).
[19] V. V. Moshchalkov, M. Baert, V. V. Metlushko, E. Rosseel, M. J. Van Bael, K. Temst, and Y. Bruynseraede, Phys. Rev. B **57**, 3615 (1998).
[20] M. J. Van Bael, L. Van Look, M. Lange, K. Temst, G. Güntherodt, V. V. Moshchalkov, and Y. Bruynseraede, Physica C **341-348**, 965 (2000).
[21] D. J. Morgan and J. B. Ketterson, J. Low Temp. Phys. **122**, 37 (2001).